Suppression of ripples on ablated Ni surface via a polarization grating

Hideo Iwase[1], **Satoshi Kokubo**[1], **Saulius Juodkazis**[2], **and Hiroaki Misawa**[2]

[1] *Production Engineering Headquarters, Canon Inc., Kawasaki-shi, Kanagawa 212-8602, Japan*

[2] *Research Institute for Electronic Science, Hokkaido University, CRIS Bldg., Sapporo 001-0021, Japan*

iwase.hideo@canon.co.jp; saulius@es.hokudai.ac.jp

Abstract: Gratings were recorded on the surface of nickel by ablation without formation of ripples using an interference of two p-polarized femtosecond laser beams at a $\pi/4$ angle of incidence. The mechanism of ripples' suppression is explained by formation of a polarization grating and by ablation at the locations where the polarization is normal to the Ni surface. The aspect ratio of the ablated grooves was ~ 3 with the period ~ 570 nm at the central wavelength of irradiation of 800 nm. This method is applicable for laser structuring of different materials and a recorded grating structure can be scaled with the irradiation wavelength.

OCIS codes: (140.3390) Laser materials processing; (160.3900) Metals; (220.4000) Microstructure fabrication.

References and links

1. M. J. Birnbaum, "Semiconductor surface damage produced by ruby lasers," J. Appl. Phys. **36**, 3688–3689 (1965).
2. J. F. Young, J. S. Preston, H. M. van Driel, and J. E. Sipe, "Laser-induced periodic surface structure. II. Experiments on Ge, Si, Al, and brass," Phys. Rev. B **27**, 1155 – 1172 (1983).
3. D. Emmony, R. Howson, and L. Willis, "Laser mirror damage in germanium at 10.6 μm," Appl. Phys. Lett. **23**, 598–600 (1973).
4. Q. Wu, Y. Ma, R. Fang, Y. Liao, and Q. Yu, "Femtosecond laser-induced periodic surface structure on diamond film," Appl. Phys. Lett. **82**, 1703 – 1705 (2003).
5. D. Bäuerle, *Laser processing and chemistry* (Springer, Berlin, 2000).
6. G. Miyaji and K. Miyazaki, "Origin of periodicity in nanostructuring on thin film surfaces ablated with femtosecond laser," Opt. Express **16**, 16265–16271 (2008).
7. W. Kautek, P. Rudolph, G. Daminelli, and J. Krüger, "Physico-chemical aspects of femtosecond-pulse-laser-inducedsurface nanostructures," Appl. Phys. A **81**, 65–70 (2005).
8. Y. Shimotsuma, P. G. Kazansky, J. Qiu, and K. Hirao, "Self-Organized Nanogratings in Glass Irradiated by Ultrashort Light Pulses," Phys. Rev. Lett. **91**, 247405/1–4 (2003).
9. V. R. Bhardwaj, E. Simova, P. P. Rajeev, C. Hnatovsky, R. S. Taylor, D. M. Rayner, and P. B. Corkum, "Optically Produced Arrays of Planar Nanostructures inside Fused Silica," Phys. Rev. Lett. **96**, 057404/1–4 (2006).
10. D. Wortmann, J. Gottmann, N. Brandt, and H. Horn-Solle, "Micro- and nanostructures inside sapphire by fs-laser irradiation and selective etching", Opt. Express **16**, 1517–1522 (2008).
11. S. Juodkazis, N. Kujime, H. Okuno, V. Mizeikis, S. Matsuo, and H. Misawa,"Towards nanostructuring of materials by ripples" *in Proc. of Joint Int. Workshop CREST& QNN'03*, Jul. 21-23, 2003; Awaji, Japan, 117–121 (2003).
12. J. E. Sipe, J. F. Young, J. S. Preston, and H. M. van Driel, "Laser-induced periodic surface structure. I. Theory," Phys. Rev. B **27**, 1141 – 1154 (1983).
13. A. E. Siegman and P. M. Fauchet, "Stimulated Wood's anomalies on laser- illuminated surfaces," IEEE J. Quant. Electr. **QE-22**, 1384 – 1403 (1986).

#104927 - $15.00 USD Received 5 Dec 2008; revised 4 Feb 2009; accepted 6 Feb 2009; published 4 Mar 2009

14. S. E. Clark and D. Emmony, "Ultraviolet-laser-induced periodic surface structures," Phys. Rev. B **40**, 2031–2041 (1989).
15. S. A. Akhmanov, V. I. Emel'yanov, N. I. Koroteev, and V. N. Seminogov, " Effect of high-intensity laser irradiation onto surfaces of semiconductirs and metals: optical nonlinear effects and nonlinear optical diagnostics," Sov. Phys. Usp. **28**, 675–745 (1985).
16. X. J. Wu, T. Q. Jia, F. L. Zhao, M. Huang, N. S. Xu, H, Kuroda, and Z. Z. Xu, "Formation mechanisms of uniform arrays of periodic nanoparticles and nanoripples on 6H-SiC crystal surface induced by femtosecond laser ablation," Appl. Phys. A **86**, 491–495 (2007).
17. T. Tomita, K. Kinoshita, S. Matsuo, and S. Hashimoto, "Effect of surface roughening on femtosecond laser-induced ripple structures," Appl. Phys. Lett. **90**, 153115 (2007).
18. H. Morikami, H. Yoneda, K.-I. Ueda, and R. M. More, "Detection of hydrodynamic expansion in ultrashort pulse laser ellipsometric pump-probe experiments," Phys. Rev. E **70**, 035401(R)/1–3 (2004).
19. P. Günter and J.-P. Huignard, *Photorefractive materials and their applications 1: basic effects* (Springer, New York, 2006).
20. S. Juodkazis, V. Mizeikis, and H. Misawa, "Three-dimensional structuring of resists and resins by direct laser writing and holographic recording," Adv. Polym. Sci. **213**, 157–206 (2008).
21. F. Brunel, "Not-so-resonant, resonant absorption ," Phys. Rev. Lett. **59**, 52 - 55 (1987).
22. E. G. Gamaly, N. R. Madsen, M. Duering, A. V. Rode, V. Z. Kolev, and B. Luther-Davis, "Ablation of metals with picosecond laser pulses: evidence of long-lived nonequilibrium conditions at the surface," Phys Rev. B **71**, 174405/1-12 (2005).
23. K. Hatanaka, T. Ida, H. Ono, S.-I. Matsushima, H. Fukumura, S. Juodkazis, and H. Misawa, "Chirp effect in hard X-ray generation from liquid target when irradiated by femtosecond pulses," Opt. Express **16**, 12650–12657 (2008).
24. H. Wang, L. Shi, B. Luk'yanchuk, C. Sheppard, and C. T. Chong "Creation of a needle of longitudinal polarized light in vacuum using binary optics," Nature Photonics **2**, 501–505 (2008).
25. S. Juodkazis, H. Misawa, O. A. Louchev, and K. Kitamura, "Femtosecond laser ablation of chalcogenide glass: explosive formation of nano-fibers against thermo-capillary growth of micro-spheres," Nanotechnology **17**(19), 4802 – 4805 (2006).
26. S. P. Gorkhali, S. G. Cloutier, and G. P. Crawford, and R. A. Pelcovits, "Stable polarization gratings recorded in azo-dye-doped liquid crystals," Appl. Phys. Lett. **8**, 251113 (2006).
27. H. Ono, A. Emoto, F. Takahashi, N. Kawatsuki, and T. Hasegawa, "Highly stable polarization gratings in photocrosslinkable polymer liquid crystals," J. Appl. Phys. **94**, 1298–1302 (2003).
28. T. Hashimoto, S. Juodkazis, and H. Misawa, "Void formation in glass," New. J. Phys. **9**, 253 /1–9, (2007).
29. K. Yamasaki, S. Juodkazis, S. Matsuo, and H. Misawa, "Three-dimensional micro-channels in polymers: one-step fabrication," Appl. Phys. A: Mat. Sci. & Proc. **77**, 371 - 373 (2003).
30. S. Juodkazis, K. Yamasaki, V. Mizeikis, S. Matsuo, and H. Misawa, "Formation of embedded patterns in glasses using femtosecond irradiation," Appl. Phys. A: Mat. Sci. Proc. **79**, 1549-1553 (2004).

1. Introduction

Formation of ripples [1] on surfaces of metals [2], semiconductors [1, 3], and dielectrics [4] irradiated by laser pulses/beams is a phenomenon reflecting complex light-matter interaction mechanisms: formation of surface electromagnetic waves (SEW) [5], plasmon-polaritons [6], melting, evaporation, and re-solidification governed by highly nonlinear processes driven by surface capillary waves, surface tension, and surface energy [7]. Depending on materials' optical (the dielectric function), thermodynamical (temperature of phase transitions, latent heat, thermal conductivity, etc.), mechanical properties and environment gas or liquid very different surface morphologies were observed. Recently, ripple formation inside dielectric materials were reported, where an interface of two materials with very different optical properties were created by a strong ionization and dielectric breakdown using focused ultra-short (sub-1 ps) pulses [8–10]. Laser pulses shorter than typical time of phonon equilibration and electron-ion energy exchange in ablation plasma ($\sim 1-10$ ps) are prospective for an efficient energy delivery to the irradiated surface (or volume in the case of transparent materials), since plasma screening effects are not affecting conditions of beam/pulse propagation. However, even with ultra-short pulses a high-precision and fidelity surface structuring with feature sizes comparable with the wavelength, λ, is a challenging task due to formation of ripples. Formation and self-organization of the ripples on the irradiated surfaces is still not well-controlled.

#104927 - $15.00 USD Received 5 Dec 2008; revised 4 Feb 2009; accepted 6 Feb 2009; published 4 Mar 2009

Here, we demonstrate the use of polarization grating for suppression of ripples' formation. Gratings with sub-micrometer period have been recorded on a nickel surface by ablation using the polarization grating. The depth of the ablated groove was comparable with λ and the aspect ratio on the ablation pit was approximately 2.8 (the depth to width ratio). The mechanism of laser ablation in the case of an uniform irradiance with a polarization grating is discussed. The ablation of surfaces by a normal component of the light E-field has been responsible for efficient ablation and suppression of ripples' formation.

2. Experimental

Two femtosecond laser pulses of 130 fs duration at the central wavelength of 800 nm (Spitfire, Spectra Physics) were focused on the surface of Ni samples by lenses of $f = 250$ mm focal length. The polarization of each beam was controlled by a zero-order $\lambda/2$-plate and a delay line was used to fulfill a temporal overlap of laser pulses on the surface.

Surface roughness of the Ni samples used in experiments was less than 1 nm (a min-max value). A high temperature of Ni melting 1453°C facilitates a high-precision processing of surface due to fast thermal quenching when ablation is carried out by femtosecond laser pulses at room conditions. The complex dielectric constant of Ni samples was measured by ellipsometry at cw-illumination conditions, $\varepsilon = (2.27 + 3.27\imath)^2$.

The ablated regions were observed by field-emission scanning electron microscopy (SEM). Numerical simulations of the polarization grating were carried out by a three-dimensional finite differences time domain (3D-FDTD) software package Lumerical.

3. Theory

3.1. The efficacy maps of ripple formation

The formation of ripples (also known as radiation reminants [12], stimulated Wood's anomalies [13], laser-induced periodic surface structures (LIPSS) [14]) can be described by the efficacy factor, η [12]. This factor represents an inhomogeneous absorption as a function of direction and spatial frequency on the irradiated surface. It has been demonstrated that ripples with the wavevectors approximately equal to $k_0 = 2\pi/\lambda$ can be found on surfaces of metals, semiconductors, and dielectrics [5]. Also, the ripples with very different values and directions of wavevectors can be found on the ablated surfaces [15]. The formation mechanisms of the ripples are still actively debated [7, 16, 17].

The efficacy factor can be presented as an efficacy map $\eta(\mathbf{k}, \varphi)$ [4], where φ is the angle between the wavevector $\mathbf{k}$ of SEW and the surface projection $\mathbf{k}_i = \mathbf{k}_0 \sin\theta$ of the incident wavevector $\mathbf{k}_0$ with θ being the angle of incidence. Such maps help to account for the predicted orientation and period of ripples on the surfaces [11]. Here, we will present the main formulae required to calculate such ripples maps according to the theory presented in Ref. [12].

A Fourier component of the surface roughness with a wavevector $\mathbf{k}$ scatters the impinging light with $\mathbf{k}_i$ into the surface waves according to $\mathbf{k}_\pm = \mathbf{k}_i \pm \mathbf{k}$. The intensity of the light at the pre-surface region caused by such scattering is expressed as:

$$I(\mathbf{k}) \propto \eta(\mathbf{k}, \mathbf{k}_i) \times |b(\mathbf{k})|, \tag{1}$$

where η is the efficacy factor and $b(\mathbf{k})$ is an amplitude of the surface roughness at the spatial frequency given by $\mathbf{k}$. In general, the factor η has sharp peaks when

$$|\mathbf{k}_i \pm \mathbf{k}| = \begin{cases} k_0, & \text{if } |\varepsilon| \gg 1 \\ k_0 n, & \text{if } n \simeq 1 \end{cases} \tag{2}$$

#104927 - $15.00 USD Received 5 Dec 2008; revised 4 Feb 2009; accepted 6 Feb 2009; published 4 Mar 2009

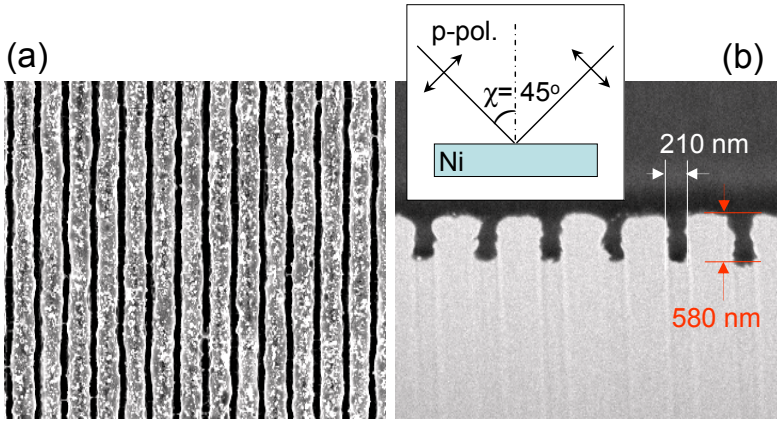

Fig. 1. SEM top (a) and cross-sectional (b) images of Ni sample after ablation by two-beam interference pattern. Geometry of experiment is shown in the inset of the panel (b). The central wavelength was $\lambda_0 = 800$ nm, pulse duration 130 fs, exposure time $1/6$ s at 1 kHz repetition rate; the number of pulses was $N = 160$. Period of ablation pattern was $\Lambda = \lambda_0/(2\sin\theta) \simeq 566$ nm. The incident power of the beams was 6.0 μJ/pulse and the ablated area was around 30 μm in diameter. The cumulative irradiance was approximately 10% above the threshold of ablation.

where $\varepsilon = (n + \kappa\imath)^2$ is the complex dielectric constant. The first case applies for typical metals, semiconductors, and dielectrics with high refractive indices, while the second for glasses and plastics in visible-to-near-IR spectral range. In order to evaluate numerically the efficacy factor is expressed as

$$\eta(\mathbf{k}, \mathbf{k}_i) = 2\pi |v(\mathbf{k}_+) + v^*(\mathbf{k}_-)|, \tag{3}$$

where the definition of function $v(\mathbf{k})$ for s- and p-polarizations with all other parameters are gathered in the appendix; here, * denotes a complex conjugate.

Though given by a cumbersome expression, the efficacy factor, η, (Eq. 3 and the appendix) can be easily calculated. Also, the local electrical field enhancement factors due to geometrical and plasmonic effects [6, 20] can be accounted for by the factor $b(\mathbf{k})$ in Eq. 1. It is noteworthy, that the real part of the dielectric function of metals can increase 1–3 times during a sub-1 ps pulse at the high-irradiance ($\sim$TW/cm^2) before onset of surface ablation and hydrodynamic movement, while the imaginary part stays almost unchanged [18]. This affects the period of ripples according to Eq. 2 and ripples of a smaller period can be imprinted on the surface.

3.2. *Polarization grating*

Here, we define the intensity distribution in a polarization grating. Two p-polarized beams at a mutual coincidence angle of 2θ create an energy density, w, distribution over the illuminated surface governed by the interference tensor, Δm, [19]:

$$w = w_0(1 + |tr\Delta m| \cos(Kx)) \tag{4}$$

where $w_0 = w_A + w_B$ is the unmodulated energy density distribution given by a superposition of the corresponding energy densities of beams A and B, $K = 2\pi/\Lambda$ is the wavevector of the

#104927 - $15.00 USD Received 5 Dec 2008; revised 4 Feb 2009; accepted 6 Feb 2009; published 4 Mar 2009

grating, x is the coordinate, tr is the trace of the matrix, and Δm [19]:

$$\Delta m = \frac{2A_A A_B}{A_A^2 + A_B^2} \begin{pmatrix} \cos^2\theta & 0 & \frac{1}{2}\sin 2\theta \\ 0 & 0 & 0 \\ -\frac{1}{2}\sin 2\theta & 0 & -\sin^2\theta \end{pmatrix}, \tag{5}$$

where $A_{A,B}$ are the field amplitudes of the two beams. Then the energy density modulation is $\Delta w = 2\sqrt{w_A w_B}(\cos^2\theta - \sin^2\theta)$; in the case considered here $\theta = \pi/4$ and one would find no intensity (energy density) modulation, since $\Delta w = 0$.

4. Results and discussion

Figure 1 shows morphology of the ablation pattern recorded on the surface of Ni sample by $N = 160$ laser pulses. The cumulative irradiance per pulse was only 10% larger than the threshold of ablation. The grooves which have the depth up to 580 nm and the width of 210 nm (the aspect ratio of 2.8) were formed on the surface. There were some debris on the surface, however, there were no any ripples which usually deteriorate the surface quality. The period of the pattern was following an expected pattern for the polarization grating $\Lambda = \lambda_0/(2\sin\theta) \simeq 566$ nm; note, there were no intensity/irradiance grating over the irradiation spot. The formed polarization gratings are expected to follow the calculated intensity pattern shown in Fig. 2(a) [26, 27]. The intensity distribution $|\mathbf{E}|^2$ has unmodulated Gaussian distribution as demonstrated in Sec. 3.2. However, the intensity components E_x^2 and E_y^2 show grating modulation as calculated by 3D-FDTD for our experimental conditions (Fig. 2(b)). A $\Lambda/2$ shift exists between the two perpendicular polarization gratings in a lateral direction as visualized in Fig. 2(b).

In order to understand the mechanism of pattern formation and ripples' suppression, Ni samples were irradiated by a small ($N = 5-15$) number of pulses in order to detect the onset of pattern formation. Irradiation was carried out for s- and p-polarized pulses, respectively. The results are summarized in Fig. 3. In the case of s-polarization (a), a complex pattern of ripples emerged. Note, in this case there was an intensity grating formed (in contrast to the case of interference of p-polarized pulses). The efficacy factors (Eq. 3) are plotted for the ripples whose wavevectors are parallel ($\varphi = 0^\circ$) and perpendicular ($\varphi = 90^\circ$) to the plane of incidence; the latter are sometimes called anomalous ripples. The ripples aligned in these two specific directions were most prominent on the ablated Ni surfaces (Fig. 3(a)). The peaks, dips, or kinks in the efficacy plot reflects the light intensity re-distribution on the irradiated surface and is usually imprinted on the surface in the form of ripples. There is a strong correlation between the efficacy map and ripples on the surface [2, 12] as we also observed and discuss below.

The periods of ripples corresponding to the two spilt peaks $peak_1^P$ and $peak_2^P$ in the efficacy maps (Fig. 3(b)) are given by $\Lambda_\pm(\theta) = (1/\Lambda_0 \pm \sin\theta/\lambda_0)^{-1}$ where Λ_0 is a spacing at $\theta = 0^\circ$ [5]. The spacings and running directions of the $R^s_{\varphi=0^\circ}$ and $R^s_{\varphi=90^\circ}$ ripples is shown in Fig. 3 and is in good agreement with the positions of the $edge^s$ and dip^s efficacy features marked in the corresponding efficacy map. The ripples $R^s_{\varphi=90^\circ}$ were considerably more expressed than those marked $R^s_{\varphi=0^\circ}$, in a good correspondence with theory, i.e., the sharp dip, dip^s, was causing formation of the $R^s_{\varphi=90^\circ}$ ripples and the less expressed ripples $R^s_{\varphi=0^\circ}$ were due to a weaker $edge^s$ feature in the efficacy map (a).

The periodic structure corresponding to the $peak_3^p$ in the efficacy plot (Fig. 3(b)) was distinguishable as ripples $R^p_{\varphi=90^\circ}$ (b). When Ni surface was irradiated with imperfectly overlapped p-polarized beams the ripples with period $R^p_{\varphi=0^\circ}$ (the inset in Fig. 3(b)) were also found in accordance with $peak_1^p$ of the efficacy plot. The ripples $R^p_{\varphi=90^\circ}$ remained on the bottom of the structures after large number of pulses (e.g., Fig. 1), however, they had no detrimental influence on the overall formation of the ablated grating of the period $\Lambda \simeq 566$ nm. The predictions of ablation efficacy plots for the normal incidence of 800 and 400 nm (not shown here) wavelengths

#104927 - $15.00 USD Received 5 Dec 2008; revised 4 Feb 2009; accepted 6 Feb 2009; published 4 Mar 2009

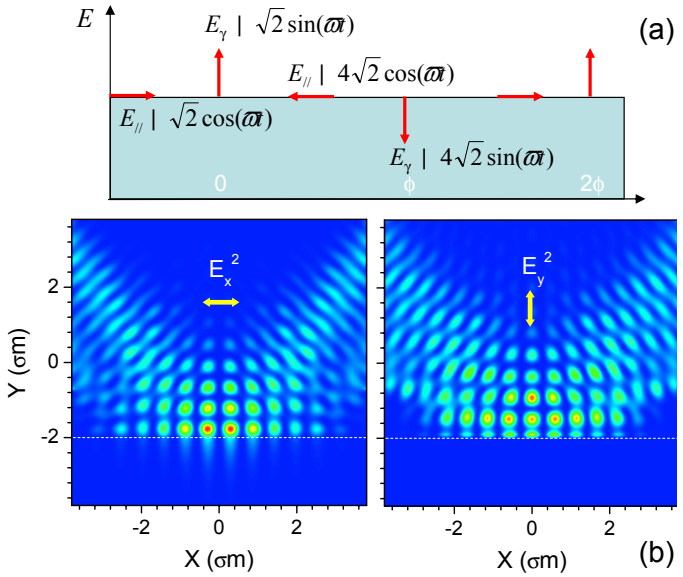

Fig. 2. (a) The polarization grating formed by interference of two p-polarized beams (see, the inset of Fig. 1(b)) at the mutual incidence angle of $2\theta = \pi/2$. The E-field components perpendicular and parallel to the surface are marked as $E_\perp$ (or E_y) and $E_\parallel$ (E_x), respectively; ω is the cyclic frequency and t denotes time (see, Eq. 5). (b) The 3D-FDTD calculation of the $|E_{x,y}|^2$ intensity distribution of Gaussian beams on the surface of a metal (gold was used for the perfect metal) for the experimental conditions shown in (b). The dashed line in (b) shows location of surface; the intensity maxima are 4.7 and 4 for the E_x^2 and E_y^2 components, respectively (the amplitude of the incident field is $|E_{in}| = 1$).

fs-laser pulses were satisfactorily corresponding to the experimentally observed ablation patterns.

The mechanism of Ni ablation in the case of a spatially unmodulated Gaussian intensity distribution when the polarization grating is present is discussed next. The locations where E-field is oscillating perpendicularly to the Ni surface (Fig. 2(b)) at the irradiation intensity slightly above the threshold of ablation are the regions where ionization is most expected. Indeed, electrons can be freed from surface states and accelerated in close proximity to the sample's surface. In the oscillating E-field, those pre-surface electrons are forced back into the surface during every half of an optical cycle. The ionization and heating via inverse bremstahlung become more efficient at these locations; this is known as a Brunel or vacuum heating mechanism [21]. Such spatially localized heating leads towards efficient ablation, i.e., ions are departing from the surface when their energy (defined by temperature) is larger than the binding energy of solid, which is typically few electronvolts [22]. The air ambience is facilitating the ablation via direct ion departure as well as evaporation from the metal surface as has been demonstrated earlier [22]. In case of multi-pulse exposure, formation of nano-droplets and trenches is expected at those particular locations were material starts to ablate. They cause a further enhancement of the E-field via the geometrical local field factor and, consequently, the ionization becomes even more efficient [20]. This establishes a positive feedback mechanism and promotes self-organized formation of the pattern, which has a period defined by the polarization grating despite the uniform intensity distribution.

It is well known that, namely, p-polarization is required for the hard X-ray generation by fem-

#104927 - $15.00 USD Received 5 Dec 2008; revised 4 Feb 2009; accepted 6 Feb 2009; published 4 Mar 2009

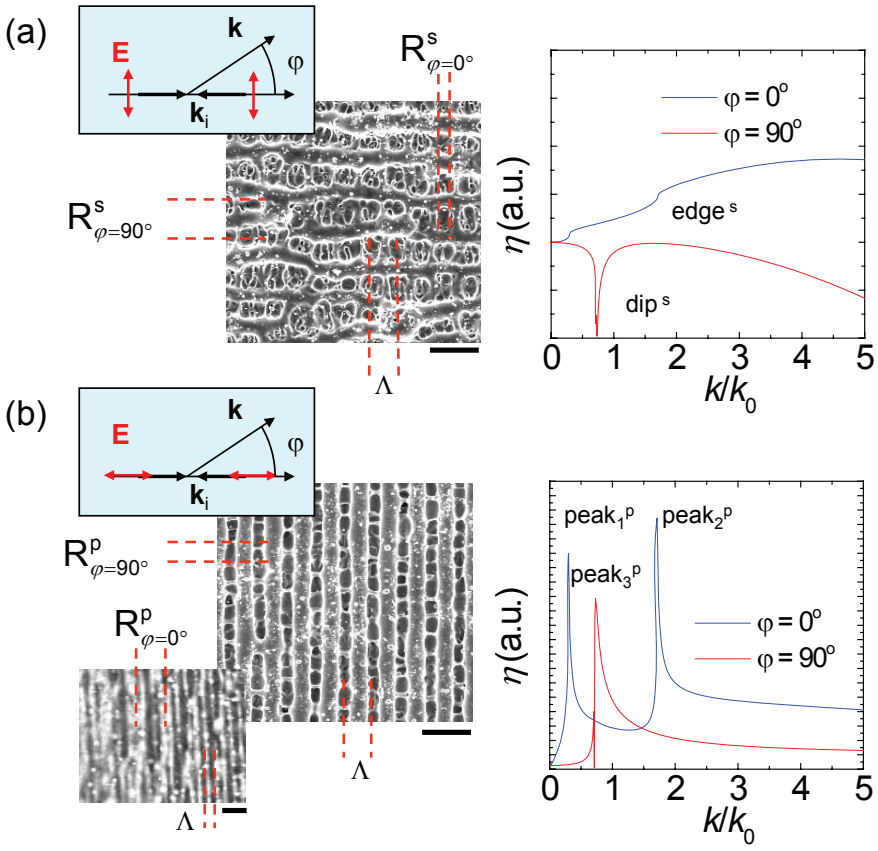

Fig. 3. SEM images of the ablated Ni surface and the efficacy factors (Eq. 3) for s- (a) and p-polarizations (b), respectively. The angle of incidence was $\theta = 45^\circ$ (the corresponding period of the gratings is $\Lambda = \lambda_0/(2\sin\theta) \simeq 566$ nm); the surface projection of polarizations and wavevectors are schematically shown in the insets; φ is the angle on the sample's surface out of the plane of incidence (out of x-axis). The number of pulses was $N < 15$ at the cumulative irradiance 10% above the ablation threshold. SEM image of the Ni surface ablated by imperfectly overlapped p-pol. beams is shown as the lower inset in (b). Scale bars are 1 μm. Optical parameters used for estimation of η are $n = 2.27$, $\kappa = 3.27$, and geometrical parameters $F = 0.1$, $s = 0.4$. See, text and Appendix for details.

tosecond laser pulses due to the presence of an E-field component normal to the surface (see, e.g., [23]). This component is more efficient in heating and ionization of the surface and pre-surface plasma as compared to the s-polarization (parallel to the surface). The physical reason of the more effective electron and plasma heating by a normal component is that the electrons oscillating in that field would not screen the incoming light and light energy could be efficiently delivered to the surface at those locations. It was recently suggested to use vertical polarization for surface nano-structuring [24]. Obviously, the melting and re-solidification processes occurring dynamically in the presence of strong temperature and surface tension gradients are affecting the final morphology of the ablated patterns [5, 25]. However, the high melting temperature of Ni, low laser repetition rate, and ultra-short pulses were important to reduce the influence of thermo-capillary phenomena, which were observed in the in-bulk damage of glasses [28]. The

#104927 - $15.00 USD Received 5 Dec 2008; revised 4 Feb 2009; accepted 6 Feb 2009; published 4 Mar 2009

normal E-field component above the ablation threshold facilitates ionization, plasma formation, and removal of material without triggering SEWs or surface plasmon-polaritons. The polarization grating with the horizontal component (Fig. 2(b)) could still launch SEWs and generate ripples, however, due to a small available length $< \Lambda$ of flat surface for SEWs (at the locations were E-field is parallel to the surface) and due to the changing projection k_i over the irradiated surface the formation of ripples was not efficient and was not observed experimentally.

The qualitative explanation of the ripple suppression as a result of surface ionization in the field of vertical (to the surface) E-field component is in a good agreement with the experimental observations. The ablation grooves had a distinctive rectangular cross section (Fig. 1), which is different from typical ablation ripples which have aspect ratio close to one with a harmonic cos-form cross-section. The rectangular cross section of ablated pattern might be caused by auxiliary ripples formed on the vertical side-walls of the grooves (see, Fig. 1(b)) and will be studied next. Indeed, the vertical side-walls are parallel to the vertical E-field component and ripples with wavevector parallel to the field can be formed. A controlled surface nano-structuring by high-aspect-ratio grooves was the most efficient at a pre-threshold irradiance due to reduced melting and evaporation. The discussed mechanism based on ionization and Brunel heating is applicable for surfaces of different materials including semiconductors and dielectrics and is expected to be less efficient in the case of an in-bulk laser structuring [29, 30] due to absence of free surfaces. The proposed method of grating fabrication by creation of the vertically (to the surface of target) polarized E-field component is scalable with the wavelength.

5. Conclusions

The method of ripples' suppression on the surface of Ni is demonstrated using a two-beam irradiation geometry for creation of the polarization grating (without intensity grating) over the irradiation spot. This technique could be used for recording of sub-micrometer gratings on the surfaces of different materials and can be scaled with the irradiation wavelength. Surface ablation in the normal E-field component explains the observation.

Appendix

The expressions of $v(\mathbf{k}_\pm)$ for the s- and p-polarization used in evaluation of Eq. 3 are gathered here [12]:

$$v(\mathbf{k}_\pm) = [h_{ss}(k_\pm)(\mathbf{k}_\pm \cdot \mathbf{x})^2 + h_{kk}(k_\pm)(\mathbf{k}_\pm \cdot \mathbf{y})^2]\gamma_t |t_s(\mathbf{k}_i)|^2 \quad (\text{for s}-\text{pol.}), \tag{6}$$

$$\begin{aligned} v(\mathbf{k}_\pm) = {} & [h_{ss}(k_\pm)(\mathbf{k}_\pm \cdot \mathbf{y})^2 + h_{kk}(k_\pm)(\mathbf{k}_\pm \cdot \mathbf{x})^2]\gamma_t |t_x|^2 + h_{kz}(k_\pm)(\mathbf{k}_\pm \cdot \mathbf{x})\gamma_z \varepsilon t_x^* t_z \\ & + h_{zk}(k_\pm)(\mathbf{k}_\pm \cdot \mathbf{x})\gamma_t t_z^* t_x + h_{zz}(k_\pm)\gamma_z \varepsilon |t_z|^2 \quad (\text{for p}-\text{pol.}), \end{aligned} \tag{7}$$

where $\mathbf{x}$ and $\mathbf{y}$ are the unity vectors along the corresponding coordinate, $t_x = w(k_i)t_p(k_i)/(k_0 n)$ and $t_z = k_i t_p(k_i)/(k_0 n)$ with the following parameters:

$$h_{ss} = 2\imath k_0 (w_0 + w)^{-1} \tag{8}$$

$$h_{kk} = 2\imath w_0 w k_0^{-1} (w_0 \varepsilon + w)^{-1} \tag{9}$$

$$h_{zz} = 2\imath k^2 k_0^{-1} (w_0 \varepsilon + w)^{-1} \tag{10}$$

$$h_{zk} = 2\imath k w_0 k_0^{-1} (w_0 \varepsilon + w)^{-1} \tag{11}$$

$$h_{kz} = 2\imath w k k_0^{-1} (w_0 \varepsilon + w)^{-1} \tag{12}$$

#104927 - $15.00 USD Received 5 Dec 2008; revised 4 Feb 2009; accepted 6 Feb 2009; published 4 Mar 2009

with $w_0 = \sqrt{k_0^2 - k^2}$ and $w = \sqrt{k_0^2 \varepsilon - k^2}$; $\imath = \sqrt{-1}$. The other parameters necessary to calculate the efficacy factor are Fresnel coefficients $t_s = 2w_0(w_0 + w)^{-1}$ and $t_p = 2w_0 n(w_0 \varepsilon + w)^{-1}$, for s- and p-polarizations, respectively.

The filling factor is defined as $F = \langle b(\mathbf{k}) \rangle$ and the shape factor $s = l_t/l$, where l_t is the transverse correlation length between the random sub-micrometer trenches on the surface. It has been experimentally established that the ablation patterns on metals, semiconductors [2], and dielectrics [4] can be explained by $F = 0.1$ and $s = 0.4$. Also, the surface finishing quality was not affecting considerably the ablation pattern; hence, this set of parameters was used in our calculations (Fig. 3).

#104927 - $15.00 USD Received 5 Dec 2008; revised 4 Feb 2009; accepted 6 Feb 2009; published 4 Mar 2009